Letter

Heat conduction in magnetic insulators via hybridization of acoustic phonons and spin-flip excitations

Christopher A. Pocs,[1] Ian A. Leahy,[1] Jie Xing,[2] Eun Sang Choi,[3] Athena S. Sefat,[2] Michael Hermele,[1,4] and Minhyea Lee[1]

[1]*Department of Physics, University of Colorado, Boulder, Colorado 80309, USA*
[2]*Materials Science and Technology Division, Oak Ridge National Laboratory, Oak Ridge, Tennessee 37831, USA*
[3]*National High Magnetic Field Laboratory, Tallahassee, Florida 32310, USA*
[4]*Center for Theory of Quantum Matter, University of Colorado, Boulder, Colorado 80309, USA*

(Received 20 February 2024; revised 29 October 2024; accepted 22 January 2025; published 7 April 2025)

We present a comprehensive study on the longitudinal magnetothermal transport in a paramagnetic effective spin-1/2 magnetic insulator $CsYbSe_2$, by introducing a minimal model requiring only Zeeman splitting and magnetoelastic coupling. We use it to argue that hybridized excitations—formed from acoustic phonons and localized spin-flip-excitations across the Zeeman gap of the crystal electric field ground doublet—are responsible for a nonmonotonic field dependence of longitudinal thermal conductivity. Beyond highlighting a starring role for phonons, our results raise the prospect of universal magnetothermal transport phenomena in paramagnetic insulators that originate from simple features shared across many systems.

DOI: 10.1103/PhysRevResearch.7.L022007

Magnetic insulators provide excellent playgrounds to realize a range of exciting spin models, some of which predict exotic spin ground states. Thanks to its exclusive sensitivity to itinerant excitations, thermal conductivity is one of the most valuable probes for examining magnetic insulators and for characterizing the magnetic ground state [1–5]. The magnetic field (H) dependence of thermal transport has been argued to be a signature of unconventional spin excitations [6–12]. However, even though phonon excitations of the crystalline lattice are the dominant heat carriers, much of our understanding relies on viewing them in a subsidiary role. When phonons are not entirely neglected in studying the field-dependence of thermal conductivity, one typically considers a thermal current of phonons scattering off spin excitations. While such perspectives can be useful, they can also be oversimplifications that lead us to miss essential physics.

A case in point is the nonmonotonic field dependence of thermal conductivity (κ) that has been observed in the paramagnetic states of several effective spin-1/2 magnetic insulators. Namely, (i) $\kappa(H)$ first decreases to a minimum at $H = H_{\min}$ followed by an increase and (ii) $H_{\min}$ moves toward large values with increasing temperature. A handful of systems have shown this behavior including $Cu_3VO_7(OH)_2{\cdot}H_2O$ [7], $YbTiO_7$ [8], Cd-kapellasite [10], gadolinium gallium garnet [13], and α-$RuCl_3$ above its ordering temperature [14]. Explaining this phenomenology in terms of spin-phonon scattering alone is not plausible, without invoking unusual responses of the spin sector to applied field that seem unlikely to be present across such a wide range of systems. Instead, a generic explanation is called for that involves only common ingredients, that treats phonon and spin excitations on equal footing, and that focuses on the paramagnetic state above magnetic ordering and spin exchange temperature scales, where universal behavior can reasonably be expected.

Here, we propose such an explanation via our study of the well-characterized Kramers pseudospin-1/2 Yb- based triangular lattice $CsYbSe_2$, where we observed the nonmonotonic field dependence of κ described above. We propose that the longitudinal heat conduction under field is enabled by the hybridized quasiparticles formed from acoustic phonons and spin-flip excitations (SFEs) across the Zeeman gap, and hypothesize that the resulting hybridized excitations are responsible for the nonmonotonic $\kappa(H)$. This aligns with a highly simplified theoretical model that qualitatively reproduces key features of the experimental data. The two main ingredients of our model, namely (i) single-ion Zeeman splitting and associated SFEs and (ii) magnetoelastic (ME) coupling that mediates phonon-SFE hybridization, are common in magnetic insulators. Therefore, our results offer a starting point to understand the nonmonotonic field dependence of κ observed in a range of other systems. A quantitative theory of this field dependence will require microscopic calculations able to incorporate detailed characteristics of specific materials, and is a topic for future work.

Hybridization is an archetypical manifestation of quantum mechanics, and there is a long history of studying hybridization between phonons and different types of magnetic excitations [15], largely with a focus on spectroscopic properties. More recently, theoretical works [16–20] and one experimental study [21] have considered magnon-phonon hybridization in magnetically ordered systems, and the result-

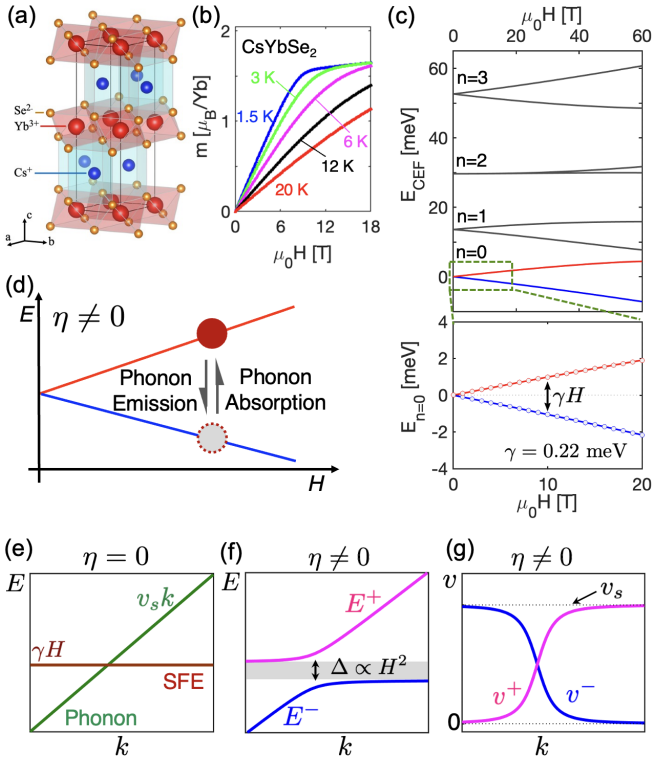

FIG. 1. (a) Crystal structure of $CsYbSe_2$: Yb^{3+} (red) forms triangular nets within the *ab* plane, formed by edge-sharing $YbSe_6$ octahedra. (b) Calculated paramagnetic single-ion magnetization within Weiss mean-field approximation [22]. (c) Field dependent crystal electric field energy spectrum calculated with the parameters in [22], where linear splitting of the ground state doublets is shown. (d) Schematic illustration of the processes leading to hybridization of phonons and SFEs, where a SFE decays (is created) by emitting (absorbing) a phonon. (e) Schematic sketch of the dispersion relation with no ME coupling ($\eta = 0$). A flat band of SFEs has energy γH, independent of wave vector k, while an acoustic phonon has a linear dispersion with slope v_s. (f) Schematic dispersion relation in the presence of nonzero ME coupling ($\eta \neq 0$), where hybridization leads to an avoided crossing and the opening of a gap between upper and lower branches of hybrid SFE-phonon excitations. (g) Group velocities $v_\pm = \frac{dE_\pm}{dk}$, derived from the dispersion of the hybridized excitations.

ing Berry phase, as a mechanism to generate a (transverse) thermal Hall signal in insulators. In contrast with these prior works, we find dramatic effects of hybridization on the easily measurable longitudinal thermal conductivity. Moreover, while the previous works on thermal Hall effect require particular magnetic orderings or specific forms of spin-spin interaction, our model relies only on ingredients present in *any* effective spin-1/2 system, namely Zeeman splitting and magnetoelastic coupling.

The Yb-based triangular-lattice compound $CsYbSe_2$ has space group $P6_3/mmc$ and consists of layers of edge-sharing $YbSe_6$ octahedra separated by Cs^{3+} ions as shown in Fig. 1(a). Millimeter-sized hexagonal shape $CsYbSe_2$ single crystals were grown by the salt flux method following the procedure described in Ref. [23]. The in-plane longitudinal thermal conductivity ($\nabla T \parallel ab$) was measured on the samples of typical dimensions $1.5 \times 3 \times 0.02$ mm^3 using a single-heater, two-thermometer configuration in steady-state operation with the field applied in the *ab* plane parallel to the thermal gradient. All thermometry was performed using Cernox resistors, which were precalibrated individually and *in situ* under the maximum applied fields of two different cryostats with superconducting magnets.

Yb^{3+} carries a $J = 7/2$ magnetic moment, which is split into four doubly degenerate crystal electric field (CEF) levels at zero field. Single-ion CEF parameters have been determined in [22], allowing for calculations of the paramagnetic magnetization within the Weiss-mean field approximation [Fig. 1(b)], which agree well with the magnetization data up to $\mu_0 H = 7$ T. The CEF energy spectrum under field was also obtained and shown in Fig. 1(c), where the Kramers doublets are split via the Zeeman effect under applied field. When temperature (T) is lowered below the first excitation energy gap ($\Delta_{10} \simeq 13$ meV), restriction of the dynamics to the ground doublet justifies use of a pseudospin-1/2 model $\mathcal{H}_Z = \gamma H \hat{S}^x$, where $\hat{S}^i$ are the pseudospin-1/2 operators, we always apply the field along the x axis (within the crystalline *ab* plane), and $\gamma = 0.22$ meV/T [22].

SFEs are excitations across the Zeeman gap, where a single pseudospin is flipped from its $S^x = -1/2$ ground state to the $S^x = +1/2$ excited state. SFEs are a kind of magnon excitation; we use the term SFE because it is more descriptive and specific for the spin excitations of our model. Without hybridization of SFEs and phonons, there is a flat band of nonpropagating SFEs [Fig. 1(e)]. Hybridization modifies the dispersion of SFEs and phonons as shown schematically in Fig. 1(f), leading to two branches of mixed excitations with nonzero group velocities [Fig. 1(g)].

The $CsYbSe_2$ system is particularly well suited to explore the hybridization of acoustic phonons and SFEs: (i) The CEF gap between the ground and first excited doublets $\Delta_{10} \approx 13$ meV provides a large T range where the effective spin-1/2 approximation is valid. (ii) The small exchange energy ($J_{ex} \approx 0.4$ meV) combined with geometric frustration prevents long-range magnetic order down to 0.3 K at zero field, with signs of field-induced local correlations below 1 K [22,24], leading to a wide paramagnetic regime where spin-spin exchange interactions may be neglected to a first approximation.

Figure 2 displays the thermal conductivity of $CsYbSe_2$ as a function of temperature $1.5\,\text{K} < T < 150\,\text{K}$ and field up to $\mu_0 H = 18$ T, within the paramagnetic state, where the temperature gradient and field are parallel and within the *ab* plane. The monotonically increasing, field-independent behavior of κ for $T \gtrsim 60$ K is not typical of crystalline materials, but similar behavior is commonly observed in nonmagnetic amorphous solids [25,26]. We note that $CsYbSe_2$ and other delafossites form crystals in very thin layers that easily become separated along the c axis, and are prone to stacking faults. We speculate this is responsible for the increasing thermal conductivity at higher temperatures. For $T < 50$ K, the T dependence of κ is affected by field, where $\mu_0 H = 14$ T enhances (suppresses) κ at low (high) temperatures as shown in Fig. 2(a). The nonmonotonic field dependence is clarified by plotting κ versus H at several values of T in Fig. 2(b). When $T < 5$ K, $\kappa(H)$ exhibits weak field dependence as H is first increased from zero, then rapidly increases upon further increasing H. As T increases above 5 K, $\kappa(H)$ shows

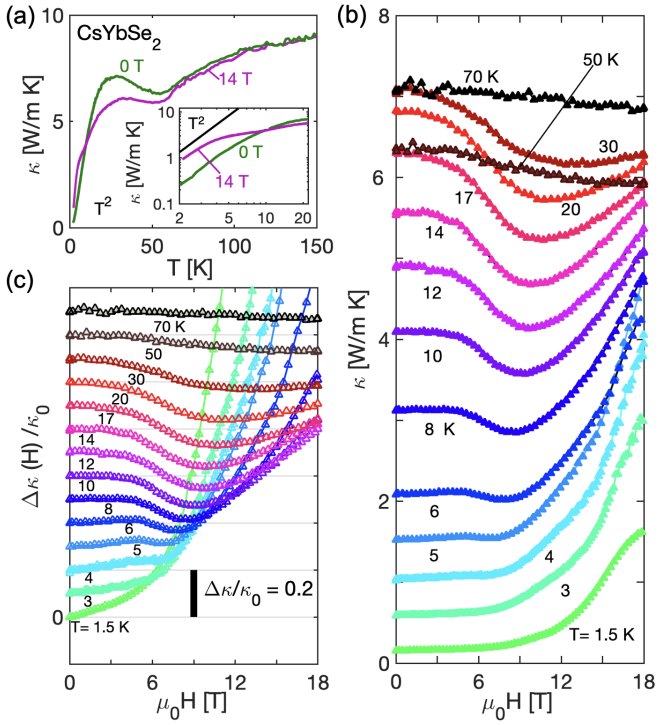

FIG. 2. (a) Temperature dependence of thermal conductivity κ at zero field and at 14 T. Inset shows the magnified view for $T <$ 20 K, where T^2-like behavior can be seen at lower temperatures. (b) Magnetic field dependence of κ is shown at various temperatures. Above $T = 5$ K, a shallow minimum of $\kappa(H)$ appears at $H = H_{\rm min}$, where $H_{\rm min}$ increases with temperature, while for $T < 5$ K, $\kappa(H)$ is characterized by a rapid increase for $\mu_0 H > 6$ T. (c) Fractional thermal conductivity $\Delta\kappa(H)/\kappa_0$ is plotted as a function of H at various temperatures with offset for clarity.

a decrease with increasing H until reaching a pronounced minimum at $H = H_{\rm min}$. The field $H_{\rm min}$ moves to large values as T increases, eventually becoming hard to locate as the field-dependence is diminished. Figure 2(c) shows the fractional thermal conductivity, defined as $\Delta\kappa(H)/\kappa_0 \equiv (\kappa(H) - \kappa_0)/\kappa_0$, where κ_0 is the value at zero field at a given T. This quantity is plotted with a constant offset along the y-axis to highlight the monotonic increase of $H_{\rm min}$ with T.

To explain the $\kappa(H)$ data of $CsYbSe_2$, we need to consider a coupling between phonons and magnetic excitations. Recalling that the CEF effect arises from electrostatic interactions between a single magnetic ion and its surrounding ligands, small lattice distortions can create a modulation of the characteristic magnetic energy scales, leading to ME coupling. For example, varying the distortion of $YbSe_6$ octahedra will change the anisotropy of the g tensor. At sufficiently low T when only the ground doublet is occupied, the most general linear ME coupling arising from local lattice distortions is $\mathcal{H}_{\rm ME} = \mu_0\mu_B \sum_{i,j} H_i \delta g_{ij} \hat{S}^j$. That is, ME coupling enters via a modulation of the g-tensor δg_{ij}. For small lattice distortions each component of δg is a linear combination of components of the symmetric strain tensor $\epsilon_{ij} = \partial_i u_j + \partial_j u_i$, where u_i is the displacement field. We note that lattice distortions do not couple to the pseudospin in the limit of zero field, where time reversal symmetry holds and Kramers theorem prevents any splitting of the ground doublet. This contrasts with non-Kramers doublet systems such as $TmVO_4$, where the ME coupling remains nonzero in vanishing applied field [27].

The most dramatic consequence of this ME coupling turns out to be the hybridization of SFEs and phonons, arising from terms corresponding to the emission/absorption processes illustrated in Fig. 1(c). Here we introduce a highly simplified effective model designed to capture the essential qualitative physics of hybridization as manifested in thermal conductivity. Our model can be motivated by a more microscopic treatment sketched in the Appendix. The SFEs are treated as bosons within a standard spin wave approximation, and we focus on only a single polarization of acoustic phonon. The energies $E_\pm(k)$ of the two branches of hybridized excitations are the eigenvalues of the matrix

$$\mathcal{H}(k) = \begin{pmatrix} \hbar v_s k & \sqrt{\eta \hbar v_s k}\gamma H \\ \sqrt{\eta \hbar v_s k}\gamma H & \gamma H \end{pmatrix}, \quad (1)$$

where v_s is the sound velocity. From specific heat in zero field (data not shown), we obtained $\hbar v_s = 12.97$ meVÅ equivalent to 1.97×10^3 m/sec and also the Debye energy $\hbar\omega_D = 7.1$ meV. The off-diagonal matrix elements arise from $\mathcal{H}_{\rm ME}$ with ME coupling strength parametrized by η. The $\sqrt{k}$ dependence matches the scaling of off-diagonal matrix elements within the treatment of the Appendix. Here, we neglect any angular dependence and assume the hybridized excitations have a spherically symmetric dispersion. The off-diagonal terms in Eq. (1) make it transparent that applied field simultaneously tunes the Zeeman gap γH and the strength of ME coupling.

The energies of hybridized quasiparticles take the form

$$E_\pm(k) = \left(\frac{E_0 + \gamma H}{2}\right) \pm \sqrt{\left(\frac{E_0 - \gamma H}{2}\right)^2 + \eta E_0 \gamma^2 H^2}, \quad (2)$$

where $E_0 = \hbar v_s k$. The dispersion of $E_\pm$ as a function of wave vector k is plotted in Figs. 3(a)–3(c) for applied fields $\mu_0 H =$ 4, 8, and 16 T, respectively. The lower branch $E_-(k)$ increases monotonically from zero to $\gamma H - \eta(\gamma H)^2$ as $k \to \infty$, while the upper branch $E_+(k)$ starts at $E_+(k = 0) = \gamma H$ and monotonically increases. The size of the gap Δ between the two branches thus takes the simple form $\Delta = \eta(\gamma H)^2$ when including states with arbitrarily large values of k. The change in gap size upon imposing the momentum cutoff $k < \pi/a$ is negligible, as illustrated by the gray shading in Figs. 3(a)–3(c); here, $a = 4.42$Å is the ab-plane lattice constant. Note that the lower branch dispersion becomes flat with $E_-(k) = 0$ when $\eta = (\gamma H)^{-1}$, signaling an instability reached either at large ME coupling or strong applied field, beyond which the model will not be valid. We thus always take $\eta < (\gamma H)^{-1}$, where $E_-(k)$ is nonzero and remains real. Figure 3(d) displays a magnified view of the low-energy region: the slope (i.e., group velocity) at $k = 0$ decreases monotonically with increasing field. This is important for determining the high field behavior, as discussed below.

SFEs are subject to a hard-core repulsive interaction that forbids two or more excitations from occupying the same lattice site. This is neglected in a naïve linear spin-wave treatment, where SEFs are represented by bosonic particles for which arbitrarily high occupation number is allowed. We

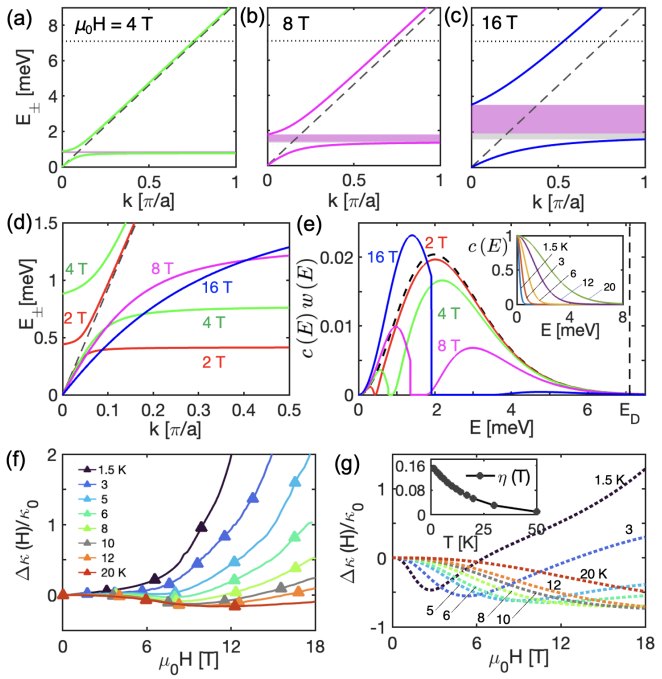

FIG. 3. [(a)–(c)] $E_\pm(k)$ of Eq. (2) are plotted for $\mu_0 H = 4, 8$, and 16 T, with $\eta = 0.13$ meV^{-1}. Dashed lines show the phonon dispersion without ME coupling, while dotted horizontal lines indicate the Debye energy $E_D = 7.1$ meV. The energy gap $\Delta \propto H^2$ between upper and lower branches is shown with pink (integrating over all k) and gray (cutoff at $k < \pi/a$) shading. (d) $E_\pm(k)$ for several values of applied field at smaller values of k. (e) The integrand $c(E)w(E)$ of Eq. (3) is shown for several values of applied field at $T = 6$ K. The upper and lower branches are clearly visible as two separate peaks separated by the gap, where $g(E) = 0$. The inset plots the specific heat $c(E)$ at selected temperatures. Comparison of (f) measured and (g) calculated $\Delta\kappa/\kappa_0$ as a function of applied field at the temperatures as shown. Inset displays the empirical $\eta(T)$. Despite the highly simplified model, the calculations capture the essence of the data: nonmonotonic field dependence with the minimum in $\kappa(H)$ at $H_{\min}$ moving to higher values as T increases.

account for the hard-core interaction at a mean-field level via temperature-dependent ME coupling $\eta = \eta(T)$, as described in the Appendix. The effect of hard-core repulsion should become more pronounced with increasing temperature due to thermally excited SFEs, and as a result $\eta(T)$ is expected to decrease with increasing T. In our calculations we employ an empirical monotonically decreasing form for $\eta(T)$, as shown in the inset of Fig. 3(g).

Thermal conductivity is computed within a Debye-Callaway model [25] using the above hybridized quasiparticle spectra:

$$\kappa(T,H) = \sum_{\sigma=\pm} \int \frac{d\boldsymbol{k}^3}{3(2\pi)^3} c(E_\sigma(\eta,k)) v_\sigma^2(\eta,k)\tau(k). \quad (3)$$

Here, $v_\pm = (1/\hbar)dE_\pm/dk$ and $c(E) = E dn_B/dT$ is the specific heat of a single bosonic mode, with $n_B(T)$ the standard Bose occupation function, and we impose the momentum cutoff $k < \pi/a$. The scattering time $\tau(k)$ can be expressed $\tau^{-1}(k) = \sum \tau_i^{-1}$, where relaxation rates add for different scattering processes (e.g., boundary, normal, and Umklapp scattering), and each τ_i is a function of k and/or T [25]. Unlike pure phonons, a detailed theory for scattering of the hybrid phonon-SFE excitations is not available. To highlight the transport implications of hybridization alone, we start by considering the simplest case of $\tau = \tau_0$ independent of k, and return to the issue of potential k dependence below.

With the k-independent relaxation time, we rewrite κ as the energy integral

$$\kappa(T,H) = \frac{\tau_0}{3}\int_0^\infty dE\, c(E) w(E), \quad (4)$$

using the density of states $g(E)$ of the hybridized excitations, where we defined the spectral weight $w(E) = v^2(E)g(E)$. In Fig. 3(e), the integrand of Eq. (4) is plotted for a few values of H at fixed $T = 6$ K. The upper and lower branches are clearly visible as two peaks separated by the gap. As the field is increased from zero, the contribution of the upper branch decreases as spectral weight moves to higher energy, while that of the lower branch increases with field. The evolution of $w(E)$ with applied field is shown in Fig. 5 of the Appendix.

The measured $\Delta\kappa/\kappa_0$ of $CsYbSe_2$ and the calculated result from Eq. (4) are shown, respectively, as a function of applied field in Figs. 3(f) and 3(g). The temperature dependence of τ plays no role, as it cancels out in the fractional thermal conductivity; again, we discuss k dependence of τ below. Our model qualitatively captures the essential characteristics of the data: nonmonotonic field dependence of κ observed for $T > 5$ K, as well as the movement of $H_{\min}$ to larger values with increasing T. As should be expected for a highly simplified model, there are discrepancies between the data and the calculations, to which we return below.

We now discuss how to understand the nonmonotonic field dependence of κ in terms of the hybridized phonon-SFE excitations based on simple arguments, independent of the details of our model. We assume relatively weak ME coupling such that $\eta\gamma H < c$, where $c < 1$ is an arbitrary dimensionless constant chosen not too close to 1; a simple perturbation theory argument shows that this condition prevents the hybridization from modifying the dispersion too strongly at large wave vector.

First, we consider the low-H regime where $\gamma H \ll k_B T$. In general, excitations contribute more strongly to κ when their energy density changes rapidly with temperature. This is dictated by the heat capacity $c(E)$ of bosonic excitations [inset of Fig. 3(e)], which appears in the integrand of Eq. (4). $c(E)$ is only weakly T dependent for $E \lesssim k_B T$ and decreases exponentially for $E \gtrsim k_B T$. As in Fig. 3(a), upon increasing H, opening the gap between upper and low branches pushes spectral weight in the upper (lower) branch to higher (lower) energies. The effect of this on κ is dominated by the upper branch, where $c(E)$ falls off rapidly with energy, and pushing spectral weight to higher energies leads to a decrease in κ, as can be seen in Fig. 3(e). On the contrary, for the energy scales in the lower branch, $c(E)$ only depends weakly on energy and hence the shift in spectral weight does not strongly affect κ.

Turning to the high-field $\gamma H \gg k_B T$ regime, only lower-branch states with $k \approx 0$ are appreciably thermally occupied, and the lower branch gives the dominant contribution to κ and hence its field dependence. Moreover, we can approximate

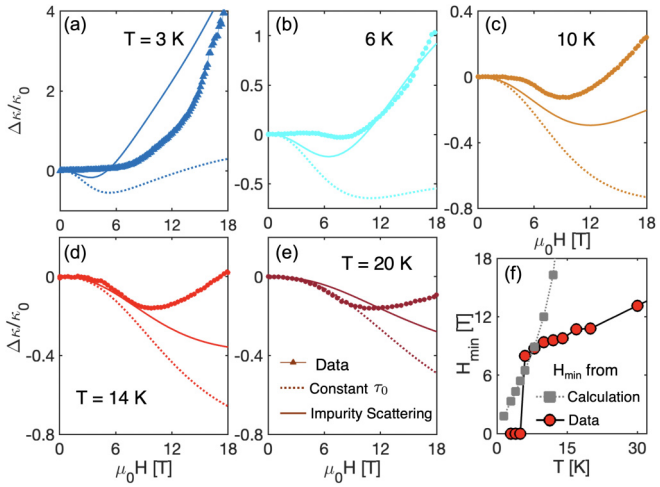

FIG. 4. [(a)–(e)] Comparison between measured (symbols) and calculated $\Delta\kappa(H)/\kappa_0$ at different T as shown. The dotted lines are from Eq. (4), the same results shown in Fig. 3(g). Solid lines are from Eq. (5) with $v_b/v_s = 0.1$. (f) $H_{\rm min}$ obtained from the impurity scattering calculation (gray squares) and data (red circles) are plotted as a function of T. Lines are connecting the symbols.

the linear dispersion $E_-(k) \approx \hbar v_{\rm eff} k$ near $k = 0$ [Fig. 3(d)]. As H increases, level repulsion bends the $k \approx 0$ lower-branch dispersion downward as illustrated in Fig. 3(b), resulting in $v_{\rm eff}$ that decreases with increasing field. Within our model, the lower-branch velocity at $k = 0$ is indeed given by $v_- = v_s - v_s\eta\gamma H$. Examining Eq. (4), one might naïvely conclude that κ should decrease as $v_{\rm eff}$ decreases, given the factor of $v(E)^2 \approx v_{\rm eff}^2$ in the integrand. However, the density of states for a linearly dispersing mode of velocity $v_{\rm eff}$ is $g(E) = E^2/2\pi^2\hbar^3 v_{\rm eff}^3$, so in fact $\kappa \propto v_{\rm eff}^{-1}$ in the high-field regime, and κ thus increases with increasing field, which is well captured in Fig. 3(g).

Finally, we discuss the discrepancies between the $\Delta\kappa/\kappa_0$ data and the calculation apparent in Figs. 3(f) and 3(g). As compared to the calculation, the data shows a more pronounced increase of $\Delta\kappa/\kappa_0$ at large applied field, and lacks the minimum in $\Delta\kappa/\kappa_0(H)$ for $T < 5$ K. These differences prompt us to consider a simple phenomenological k-dependent scattering rate $\tau^{-1} = \tau_0^{-1} + \tau_{\rm imp}^{-1}$, where τ_0 is k independent, and $\tau_{\rm imp} = \ell_{\rm imp}/v(k)$, as appropriate for scattering of hybrid phonon-SFE excitations off static impurities with a mean-free path $\ell_{\rm imp}$. Writing $\tau^{-1} = [v(k) + v_b]/\ell_{\rm imp}$, where we defined the velocity $v_b = \ell_{\rm imp}/\tau_0$, we have

$$\kappa(T,H) = \frac{\ell_{\rm imp}}{3}\sum_{\sigma=\pm}\int \frac{d^3\boldsymbol{k}}{(2\pi)^3} c(E_\sigma(k))\frac{v_\sigma^2(k)}{v_\sigma(k)+v_b}. \quad (5)$$

In the limit $v_b \gg v_\sigma(k)$, we recover our original model. In the opposite limit $v_b \ll v_\sigma(k)$, the integrand is proportional to $c(E_\sigma(k))v_\sigma(k)$ instead of $c(E_\sigma(k))v_\sigma^2(k)$.

Figures 4(a)–4(e) displays $\Delta\kappa/\kappa_0$ including impurity scattering according to Eq. (5) together with the data and calculated $\Delta\kappa/\kappa_0$ with k-independent τ_0 [Eq. (4)], at a few representative temperatures. At low T, the qualitative agreement with the data is dramatically improved, with a shallower minimum, lower $H_{\rm min}$, and a steeper rise at high field. The agreement at higher temperatures also improves, though discrepancies in detailed features still remain, as should be expected for this simplified and phenomenological model. Figure 4(f) shows the T dependence of $H_{\rm min}$ obtained from the data and from $\Delta\kappa/\kappa_0$ calculated using Eq. (5).

Needless to say, our minimal model does not account for material-specific details such as spin-spin exchange interactions, proximity to magnetic order, multiple phonon polarizations, and anisotropy in the unperturbed phonon dispersion and ME coupling, all of which may play a role. We also expect that microscopic treatments of scattering processes of the hybridized quasiparticles will bring the model closer to the observed $\Delta\kappa/\kappa_0$.

In summary, our study demonstrated that the field dependence of thermal conductivity in $CsYbSe_2$ can be attributed to heat transport by hybridized quasiparticles formed from acoustic phonons and SFEs. Our highly simplified model qualitatively captures (i) the initial decrease of κ under applied magnetic field to a minimum at $H = H_{\rm min}$, followed by an increase at higher fields and (ii) the monotonic increase of $H_{\rm min}$ with T. Including impurity scattering via a k-dependent relaxation time improves the qualitative agreement between the model and the data. The key ingredients of our model are Zeeman splitting, acoustic phonons, and weak ME coupling via modulation of the magnetic g tensor by local strain, all of which are found in many systems. We thus expect that phonon-SFE hybridization will be essential as a starting point to understand the field dependence of thermal transport in a wide range of magnetic insulators.

Acknowledgments. We thank Y. Matsuda and Y. Kasahara for helpful discussions. Work at University of Colorado Boulder was supported by the U.S. Department of Energy, Office of Science, Basic Energy Sciences (BES) under Award No. DE-SC0021377 (experimental work by C.A.P., I.A.L., and M.L.) and Award No. DE-SC0014415 (theoretical work by M.H.). Work at Oak Ridge National Laboratory (ORNL) was supported by the U.S. Department of Energy, Office of Science, Basic Energy Sciences, Materials Sciences and Engineering Division. A portion of this work was performed at the National High Magnetic Field Laboratory, which is supported by the National Science Foundation Cooperative Agreement No. DMR-1644779 and No. DMR-2128556, and the State of Florida.

Data availability. The data that support the findings of this article are openly available [28], embargo periods may apply.

Appendix: Microscopic theoretical treatment of magnetoelastic coupling. Here we sketch a more microscopic theoretical treatment of the problem of coupled acoustic phonons and SFEs, which motivates the simplified effective model described in the main text. We treat the acoustic phonons as excitations of a continuous elastic medium with displacement field $u_i(\boldsymbol{r})$ and symmetric stress tensor $\epsilon_{ij} = \partial_i u_j + \partial_j u_i$. Spin-1/2 spins $\hat{S}_{\boldsymbol{r}}^i$ lie on the sites of a Bravais lattice, and the ME coupling takes the form $\mathcal{H}_{\rm ME} = \sum_{\boldsymbol{r}} \mathcal{H}_{\rm ME}(\boldsymbol{r})$, where the sum is over lattice sites and $\mathcal{H}_{\rm ME}(\boldsymbol{r}) = \mu_0\mu_B H_x \delta g_{xi}(\boldsymbol{r})\hat{S}_{\boldsymbol{r}}^i$ as described in the main text. (In this Appendix, sums over repeated indices are implied). We drop the $i = x$ term as it does not lead to hybridization of phonons and SFEs, and the remaining terms can be written

$\mathcal{H}_{\rm ME}(\boldsymbol{r}) = \mu_0\mu_B H_x[\Lambda_{ij}\epsilon_{ij}\hat{S}^+_{\boldsymbol{r}} + \text{H.c.}]$, where Λ_{ij} is a complex matrix of coupling constants parametrizing the ME coupling and the spin raising operators are defined by $\hat{S}^+_{\boldsymbol{r}} \equiv \hat{S}^y_{\boldsymbol{r}} + i\hat{S}^z_{\boldsymbol{r}}$ [also $S^-_{\boldsymbol{r}} = (S^+_{\boldsymbol{r}})^\dagger$ for spin lowering operators]. These spin raising/lowering operators are defined to raise/lower $\hat{S}^x_{\boldsymbol{r}}$, corresponding to the direction of applied field.

To study the effect of $\mathcal{H}_{\rm ME}$, we go to momentum space. The Fourier transform of the displacement field is

$$u_i(\boldsymbol{r}) = \sum_{\boldsymbol{k},\lambda} \sqrt{\frac{\hbar}{2V\rho\omega_\lambda(\boldsymbol{k})}} e^{i\boldsymbol{k}\cdot\boldsymbol{r}} \hat{e}_{\lambda i}(\boldsymbol{k})[a_{\boldsymbol{k}\lambda} + a^\dagger_{\boldsymbol{k}\lambda}], \tag{A1}$$

where V is the volume, ρ the mass density of the crystal, and λ labels the three phonon polarizations with frequencies $\omega_\lambda(\boldsymbol{k}) = v_\lambda k$, polarization vectors $\hat{e}_\lambda(\boldsymbol{k})$, and creation operators $a^\dagger_{\boldsymbol{k}\lambda}$. Because we treat the lattice as a continuous medium, the magnitude of the wave vector $\boldsymbol{k}$ is unrestricted in the sum. For the spin operators, we define the Fourier transform by

$$S^+_{\boldsymbol{r}} = \frac{1}{\sqrt{N}} \sum_{\boldsymbol{k}\in\text{BZ}} e^{-i\boldsymbol{k}\cdot\boldsymbol{r}} S^+_{\boldsymbol{k}}, \tag{A2}$$

where N is the number of lattice sites and the wave vector sum is restricted to the first Brillouin zone.

To make a linear spin-wave approximation, we introduce Holstein-Primakoff bosons with creation operators $b^\dagger_{\boldsymbol{r}}$ by writing $S^+_{\boldsymbol{r}} = b^\dagger_{\boldsymbol{r}}\sqrt{1 - b^\dagger_{\boldsymbol{r}} b_{\boldsymbol{r}}}$. We note the form of Eq. (A2) is chosen so that if we ignore the square root and thus replace $S^+_{\boldsymbol{r}}$ by $b^\dagger_{\boldsymbol{r}}$ and $S^+_{\boldsymbol{k}}$ by $b^\dagger_{\boldsymbol{k}}$, the momentum space creation/annihilation operators satisfy canonical commutation relations. Simply dropping the square root neglects the hard-core nature of the Holstein-Primakoff bosons, but we can restore this effect at a mean-field level by replacing $S^+_{\boldsymbol{r}} \to \sqrt{1-\bar{n}}b^\dagger_{\boldsymbol{r}}$, where $\bar{n} = \langle b^\dagger_{\boldsymbol{r}} b_{\boldsymbol{r}}\rangle$.

Plugging the Fourier transforms into $\mathcal{H}_{\rm ME}$, keeping only hybridization terms proportional to $a^\dagger_{\boldsymbol{k}\lambda} b_{\boldsymbol{k}}$ (or the Hermitian conjugate), and dropping contributions from higher energy phonons outside the first Brillouin zone, we have

$$\mathcal{H}_{\rm ME} = \sqrt{1-\bar{n}}\mu_0\mu_B H_x \sum_{\boldsymbol{k}\in\text{BZ}} \sum_\lambda \left\{ \sqrt{\frac{\hbar}{2v_{\rm uc}\rho\omega_\lambda(\boldsymbol{k})}} \Lambda_{ij} \times [ik_i\hat{e}_{\lambda j}(\boldsymbol{k}) + ik_j\hat{e}_{\lambda i}(\boldsymbol{k})] a_{\boldsymbol{k}\lambda} b^\dagger_{\boldsymbol{k}} + \text{H.c.} \right\}. \tag{A3}$$

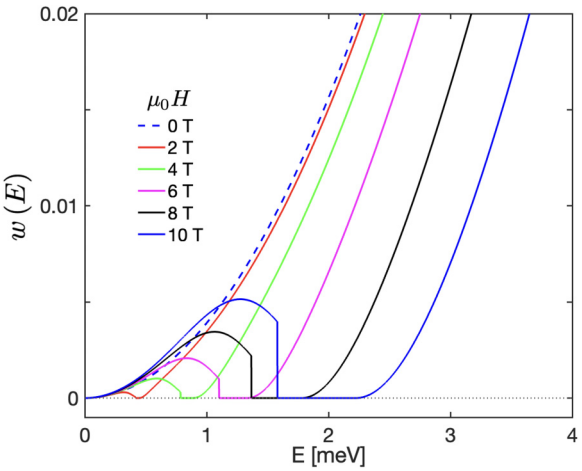

FIG. 5. The evolution of the spectral weight $w(E) = g(E)v^2(E)$ as a function of magnetic field.

Here $v_{\rm uc}$ is the volume of a crystalline unit cell. We note that the matrix elements of this Hamiltonian are proportional to $\sqrt{k}$, which comes from the factors of $k_i/\sqrt{\omega_\lambda(\boldsymbol{k})}$; this motivates the $\sqrt{k}$ dependence of the off-diagonal matrix elements in the effective model of the main text. Moreover, the effect of the mean-field correction $\sqrt{1-\bar{n}}$ is to renormalize the overall strength of the ME coupling, giving a temperature-dependent coupling that goes down as thermal occupation of SFEs increases.

Finally, we remark that it would be possible to compute κ along the same lines as in the main text using the ME coupling of Eq. (A3) and including all three phonon polarizations. While this may be valuable to explore in future work, it is important to emphasize that this introduces additional adjustable parameters associated with couplings to different phonon polarizations, significantly increasing the complexity of the model.

Spectral weight function. Figure 5 plots the spectral weight function $w(E) = g(E)v^2(E)$ as a function of E at several different magnetic field values as shown. Within the gap between upper and lower branches, $w(E) = 0$. With increasing magnetic field, the upper branch spectral weight shifts to higher energies, while the lower branch spectral weight has a peak that grows and moves to higher energies.

[1] J. Wen, S.-L. Yu, S. Li, W. Yu, and J.-X. Li, Experimental identification of quantum spin liquids, npj Quantum Mater. **4**, 12 (2019).

[2] A. V. Sologubenko, K. Giannó, H. R. Ott, U. Ammerahl, and A. Revcolevschi, Thermal conductivity of the hole-doped spin ladder system $Sr_{14-x}Ca_xCu_{24}O_{41}$, Phys. Rev. Lett. **84**, 2714 (2000).

[3] C. Hess, C. Baumann, U. Ammerahl, B. Büchner, F. Heidrich-Meisner, W. Brenig, and A. Revcolevschi, Magnon heat transport in $(Sr, Ca, La)_{14}cu_{24}o_{41}$, Phys. Rev. B **64**, 184305 (2001).

[4] S. Y. Li, L. Taillefer, C. H. Wang, and X. H. Chen, Ballistic magnon transport and phonon scattering in the antiferromagnet Nd_2CuO_4, Phys. Rev. Lett. **95**, 156603 (2005).

[5] L. Savary and L. Balents, Quantum spin liquids: A review, Rep. Prog. Phys. **80**, 016502 (2017).

[6] M. Hirschberger, J. W. Krizan, R. J. Cava, and N. P. Ong, Large thermal Hall conductivity of neutral spin excitations in a frustrated quantum magnet, Science **348**, 106 (2015).

[7] D. Watanabe, K. Sugii, M. Shimozawa, Y. Suzuki, T. Yajima, H. Ishikawa, Z. Hiroi, T. Shibauchi, Y. Matsuda, and M. Yamashita, Emergence of nontrivial magnetic excitations in a spin-liquid state of kagom volborthite, Proc. Natl. Acad. Sci. USA **113**, 8653 (2016).

[8] Y. Tokiwa, T. Yamashita, M. Udagawa, S. Kittaka, T. Sakakibara, D. Terazawa, Y. Shimoyama, T. Terashima, Y. Yasui, T. Shibauchi, and Y. Matsuda, Possible observation of

highly itinerant quantum magnetic monopoles in the frustrated pyrochlore $Yb_2Ti_2O_7$, Nat. Commun. **7**, 10807 (2016).

[9] Y. Kasahara, T. Ohnishi, Y. Mizukami, O. Tanaka, S. Ma, K. Sugii, N. Kurita, H. Tanaka, J. Nasu, Y. Motome, T. Shibauchi, and Y. Matsuda, Majorana quantization and half-integer thermal quantum Hall effect in a Kitaev spin liquid, Nature (London) **559**, 227 (2018).

[10] M. Akazawa, M. Shimozawa, S. Kittaka, T. Sakakibara, R. Okuma, Z. Hiroi, H.-Y. Lee, N. Kawashima, J. H. Han, and M. Yamashita, Thermal Hall effects of spins and phonons in kagome antiferromagnet Cd-kapellasite, Phys. Rev. X **10**, 041059 (2020).

[11] X. Hong, M. Gillig, R. Hentrich, W. Yao, V. Kocsis, A. R. Witte, T. Schreiner, D. Baumann, N. Pérez, A. U. B. Wolter, Y. Li, B. Büchner, and C. Hess, Strongly scattered phonon heat transport of the candidate Kitaev material $Na_2Co_2TeO_6$, Phys. Rev. B **104**, 144426 (2021).

[12] Q. Barthélemy, É. Lefrançois, J. Baglo, P. Bourgeois-Hope, D. Chatterjee, P. Lefloïc, M. Velázquez, V. Balédent, B. Bernu, N. Doiron-Leyraud, F. Bert, P. Mendels, and L. Taillefer, Heat conduction in herbertsmithite: Field dependence at the onset of the quantum spin liquid regime, Phys. Rev. B **107**, 054434 (2023).

[13] Y. K. Tsui, C. A. Burns, J. Snyder, and P. Schiffer, Magnetic field induced transitions from spin glass to liquid to long range order in a 3D geometrically frustrated magnet, Phys. Rev. Lett. **82**, 3532 (1999).

[14] I. A. Leahy, C. A. Pocs, P. E. Siegfried, D. Graf, S.-H. Do, K.-Y. Choi, B. Normand, and M. Lee, Anomalous thermal conductivity and magnetic torque response in the honeycomb magnet α-$RuCl_3$, Phys. Rev. Lett. **118**, 187203 (2017).

[15] V. G. Bar'yakhtar and E. A. Turov, in *Spin Waves and Magnetic Excitations*, edited by A. S. Borovik-Romanov and A. K. Sinha, Modern Problems in Condensed Matter Sciences, Vol. 22.2 (North-Holland, Amsterdam, 1988), Chap. 7, pp. 333–380.

[16] X. Zhang, Y. Zhang, S. Okamoto, and D. Xiao, Thermal Hall effect induced by magnon-phonon interactions, Phys. Rev. Lett. **123**, 167202 (2019).

[17] G. Go, S. K. Kim, and K.-J. Lee, Topological magnon-phonon hybrid excitations in two-dimensional ferromagnets with tunable Chern numbers, Phys. Rev. Lett. **123**, 237207 (2019).

[18] S. Park and B.-J. Yang, Topological magnetoelastic excitations in noncollinear antiferromagnets, Phys. Rev. B **99**, 174435 (2019).

[19] B. Ma and G. A. Fiete, Antiferromagnetic insulators with tunable magnon-polaron Chern numbers induced by in-plane optical phonons, Phys. Rev. B **105**, L100402 (2022).

[20] B. Ma, Z. D. Wang, and G. v. Chen, Chiral phonons induced from spin dynamics via magnetoelastic anisotropy, Phys. Rev. Lett. **133**, 246604 (2024).

[21] N. Li, R. R. Neumann, S. K. Guang, Q. Huang, J. Liu, K. Xia, X. Y. Yue, Y. Sun, Y. Y. Wang, Q. J. Li, Y. Jiang, J. Fang, Z. Jiang, X. Zhao, A. Mook, J. Henk, I. Mertig, H. D. Zhou, and X. F. Sun, Magnon-polaron driven thermal Hall effect in a Heisenberg-Kitaev antiferromagnet, Phys. Rev. B **108**, L140402 (2023).

[22] C. A. Pocs, P. E. Siegfried, J. Xing, A. S. Sefat, M. Hermele, B. Normand, and M. Lee, Systematic extraction of crystal electric-field effects and quantum magnetic model parameters in triangular rare-earth magnets, Phys. Rev. Res. **3**, 043202 (2021).

[23] J. Xing, L. D. Sanjeewa, J. Kim, G. R. Stewart, M.-H. Du, F. A. Reboredo, R. Custelcean, and A. S. Sefat, Crystal synthesis and frustrated magnetism in triangular lattice $CsRESe_2$ (RE = La-Lu): Quantum spin liquid candidates $CsCeSe_2$ and $CsYbSe_2$, ACS Materials Lett. **2**, 71 (2020).

[24] J. Xing, L. D. Sanjeewa, J. Kim, G. R. Stewart, A. Podlesnyak, and A. S. Sefat, Field-induced magnetic transition and spin fluctuations in the quantum spin-liquid candidate $CsYbSe_2$, Phys. Rev. B **100**, 220407(R) (2019).

[25] R. Berman, *Thermal Conduction in Solids* (Oxford University Press, Oxford, 1976).

[26] A. J. Bullen, K. E. O'Hara, D. G. Cahilla, O. Moterio, and A. v. Keudell, Topological magnon-phonon hybrid excitations in two-dimensional ferromagnets with tunable Chern numbers, J. Appl. Phys. **88**, 6317 (2000).

[27] J. K. Kjems, W. Hayes, and S. H. Smith, Wave-vector dependence of the Jahn-Teller interactions in $TmVO_4$, Phys. Rev. Lett. **35**, 1089 (1975).

[28] C. A. Pocs, I. A. Leahy, J. Xing, E. S. Choi, M. Hermele, A. S. Sefat, and M. Lee, Data for "Heat conduction in magnetic insulators via hybridization of acoustic phonons and spin-flip excitations", https://doi.org/10.25810/QA19-T327.